2020 IEEE/RSJ International Conference on Intelligent Robots and Systems (IROS)
October 25-29, 2020, Las Vegas, NV, USA (Virtual)

Accurate estimation of the position and shape of the rolling joint in hyper-redundant manipulators*

Jeongryul Kim[1], Yonghwan Moon[1,2], Seong-il Kwon[1,3], and Keri Kim[†1,3], *Member, IEEE*

***Abstract*—Hyper-redundant manipulators driven by cables are used in minimally invasive surgery because of their flexibility and small diameters. In particular, manipulators composed of many rigid links and joints have the advantages of high stiffness and payload. However, these manipulators have difficulty in estimating their positions and shapes using calculations based only on the kinematics model that assumes all joint angles are equal. In this paper, we present a method for estimating the position and shape of the rolling joint in hyper-redundant manipulators by minimizing the joint moments. This allows the determination the equilibrium position of all segments of the rolling joint, and therefore an estimation of its shape. We experimentally determine the position and shape of a prototype of the rolling joint and compare them to a simulation of our method. The maximum error between the simulation and the experimental results is 4.13 mm, which is a 77.22% improvement over the kinematic model that calculates the same joint angle. This verifies that our method accurately estimates the position and shape of the rolling joint.**

I. Introduction

Hyper-redundant manipulators (HRMs) composed of many rigid links and joints without a backbone are widely used in minimally invasive surgery (MIS) [1]. These manipulators have flexible bodies, which are advantageous in preventing damage to organs. Furthermore, manipulators driven by thin cables with redundant degrees of freedom have small diameters and bend in various directions with high stiffness and payload capacities. These advantages are fitting for medical instruments used in MIS, which requires minimal scarring to reduce surgical trauma. For these reasons, a variety of HRMs have been developed for MIS worldwide. Shang *et al*. implemented a triangular approach with two HRMs and confirmed the potential for performing surgical operations [2]. Similarly, in order to overcome the limitations of the typical endoscopic system, Thompson *et al*. demonstrated various surgical functions by operating two HRMs [3]. In addition, Degani *et al*. performed laparoscopic preclinical experiments of pigs with a snake-like, highly articulated endoscopic instrument using two concentric tubes [4]. Some researchers have studied the rolling joint mechanism since it has low buckling as well as high dexterity. In the previous study, we presented a block mechanism with a high stiffness based on a rolling joint [5]. Berthet-Rayne *et al*. proposed a snake-like robot using a rolling joint optimized in workspace, dexterity, precision and operability [6].

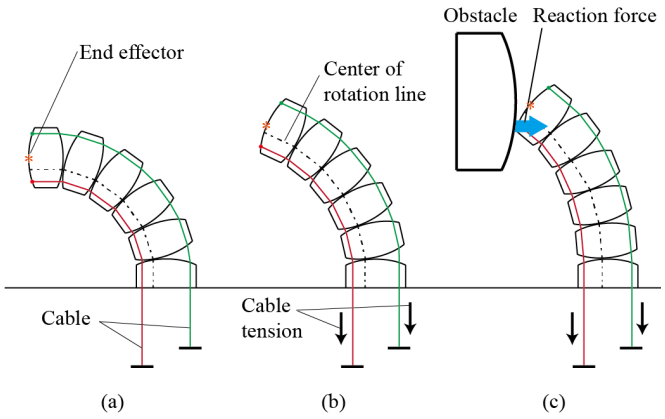

Figure 1. Concept of the bending motion of hyper-redundant manipulators (HRMs), which are composed of many rigid links and joints without a backbone. (a) Desired bent position and shape of an HRM. (b) Equilibrium position and shape of an HRM bent by cable tensions. (c) Position and shape of an HRM when it meets an obstacle.

There are several challenges to automating surgical robots using HRM. One of them is that it is difficult to predict the position and the shape of the HRM because the number of actuator cables is less than the manipulator's joint. Therefore, there is a limitation in estimating the position of the end effector and the shape of the HRM based on a kinematic model that assumes that all joint angles are equal. For example, when operators drive the HRM, they predict that the manipulator will move in a way that is similar to the kinematic model assumes all joint angles are equal. The operating cable length determines the shape and end effector position of the HRM, as shown Fig. 1(a). However, the HRM changes its actual shape and position based on the effects of the tensions and extensions of the cables, as shown in Fig. 1(b). In particular, if the manipulator meets an obstacle, the shape of the manipulator is significantly different compared to the kinematic model, as shown in Fig. 1(c). Therefore, in order to use the HRM precisely, it is necessary to analyze its actual shape and position.

*This work was supported by the Technology Innovation Program (1415162841, Development of fluorescence image guided transoral and laparoscopic single port surgery robot with flexibly articulated robotic instruments) funded by the Ministry of Trade, Industry & Energy (MOTIE, Korea).

[1]Jeongryul Kim, Yonghwan Moon, Seong-il Kwon, and Keri Kim are with the Center for Medical Robotics, Korea Institute of Science and Technology, Seoul, Korea; e-mails: jeongkim, moonyh1230, kstar1, jazzpian@kist.re.kr, respectively.

[†]Corresponding author phone: +82 29585615; fax: +82 29585304; e-mail: jazzpian@kist.re.kr.

[2]Yonghwan Moon is with School of Mechanical Engineering, Korea University, Seoul, Korea.

[3]Seong-il Kwon and Keri Kim are with the Division of Bio-Medical Science and Technology, University of Science and Technology, Daejeon, Korea.

Some researchers have estimated and simulated the movement of HRMs. Lei and Du predicted the bending curvature and path of an HRM by the kinematic model [7]. This method's weakness is that it cannot consider the change in the cable tension nor the external force on the HRM. Song *et al*. presented the shape reconstruction method based on the quadratic Bézier curves [8], and Xu *et al*. showed the deviation between the model derived by the dynamics equation and the HRM prototype [9]. Both studies found small differences between the model and the prototype. However, neither study considered external forces. Kim *et al*. demonstrated that the stiffness of the manipulator can be increased by changing the cable tension, and they also showed that the displacement decreased when the cable tension increased [10]. This study did not consider the extension of the cable at its initial position induced by the external force in the lateral direction.

In this paper, we measure the position and shape of the rolling joint of a backboneless HRM composed of many rigid links and joints as a function of bending angle. Since the object moves to the position where the sum of the force and the moment is zero, the rolling joint also moves to the equilibrium position where all joint moments are zero. The equilibrium position of the rolling joint can be derived by using the statics equation. However, it is difficult to calculate the position directly because of the nonlinearity of the rolling joint. To solve this problem, we present a method to find the equilibrium position of the rolling joint by minimizing the joint moments with forward kinematics, statics, and optimization. We use simulations to verify our experimental results for the prototype of the rolling joint.

II. METHOD

A. *Forward kinematics of the rolling joint*

We constructed a kinematic model to calculate the forward kinematics of the rolling joint. Fig. 2(a) shows two frames, $\{i_{up}\}$ and $\{i_{down}\}$, located at the centers of the rolling surfaces in the i_{th} segment. The $\{i_{up}\}$ frame is located at the center of the upper rolling surface, and the $\{i_{down}\}$ frame is located at the center of the lower rolling surface in the i-th segment. When the two segments of the rolling joint contact and rotate each other, the $\{i+1_{down}\}$ frame in the $(i+1)$th segment has a relationship with the $\{i_{up}\}$ frame in the i-th segment, as shown in Fig. 2(b). First, the distance between the frames is fixed at $2r$, where r is the radius of the rolling surface in the segment. Second, the location of the $\{i+1_{down}\}$ frame is the position rotated by $\frac{\theta_i}{2}$ over a distance of $2r$ in the $\{i_{up}\}$ frame. Third, the $\{i+1_{down}\}$ frame is rotated by θ_i relative to the orientation of the $\{i_{up}\}$ frame. Considering these relationships, we assumed two segments of the rolling joint formed a rigid arm with two revolute joints, as shown in Fig. 2(c). The first revolute joint is located at the position of the $\{i_{up}\}$ frame and rotates by $\frac{\theta_i}{2}$ over a distance of $2r$ in the link. The second revolute joint is located at the end position of the link and also rotates by $\frac{\theta_i}{2}$ at that location. From these assumptions, the position and orientation of the $\{i+1_{down}\}$ frame can be expressed in the $\{i_{up}\}$ frame. The $\{i+1_{up}\}$ frame has the same orientation as the $\{i+1_{down}\}$ frame, and is located at the distance d from the $\{i+1_{up}\}$ frame in the $-Z$ direction, as

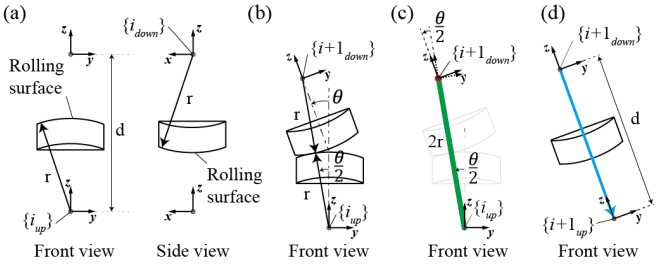

Figure 2. Schematics of the rolling joint. (a) Position and orientation of the $\{i_{up}\}$ and $\{i_{down}\}$ frames in the segment of the rolling joint (front and side views). (b) Relationship between the segments with contacts on the rolling surfaces. (c) Assumptions of the rolling joint as a two-joint rigid arm. (d) Position and orientation of the $\{i+1_{up}\}$ and $\{i+1_{down}\}$ frames.

shown in Fig. 2(d). As a result, the $\{i+1_{up}\}$ frame can be expressed in the $\{i_{up}\}$ frame with two revolute joints and one prismatic joint.

We used the Product of Exponential (PoE) formula to illustrate frames of the segment from the fixed frame $\{s\}$. The configuration of the link frame $\{i\}$ relative to the fixed frame when the mechanism is in the zero position is denoted as $M_i \in SE(3)$ and is expressed by:

$$M_i = \begin{bmatrix} R_i^M & P_i^M \\ 0 & 1 \end{bmatrix} \in SE(3). \quad (1)$$

The orientation R_i^M of M_i is the same for all segments in the $\{s\}$ frame as $R_i^M = \mathrm{diag}(1,1,1) \in so(3)$. The position P_i^M of M_i are related by $P_i^M = P_{i-1}^M + [0 \quad 0 \quad (2r-d)]^T$.

We set the odd joint of the rolling joint as the pan motion joint and the even joint as the tilt motion joint. Because the joint between the segments is assumed as the two rotate in one prismatic joint, the homogeneous transformation matrix $T_i(\theta)$ of the pan and tilt joints in the $\{s\}$ frame are derived as follows:

$$T_{2i-1}(\theta) = C_1(\theta) \cdots C_{2i-1}(\theta) M_{2i-1} \text{ at the pan point,} \quad (2)$$

$$T_{2i}(\theta) = C_1(\theta) \cdots C_{2i-1}(\theta) C_{2i}(\theta) M_{2i} \text{ at the tilt joint,} \quad (3)$$

where

$$C_{2i-1}(\theta) = e^{[s_{2i-1}^a]\frac{\theta_{2i-1}}{2}} e^{[s_{2i-1}^b]\frac{\theta_{2i-1}}{2}} e^{[s_{2i-1}^c](-d)}, \quad (4)$$

$$C_{2i}(\theta) = e^{[s_{2i}^a]\frac{\theta_{2i}}{2}} e^{[s_{2i}^b]\frac{\theta_{2i}}{2}} e^{[s_{2i}^c](-d)}, \quad i = 1, \ldots, \frac{n}{2}. \quad (5)$$

The screw axes of the joints as expressed in the $\{s\}$ frame are $S_i^a = (w_i^a, v_i^a)^T$, $S_i^b = \left(w_i^b, v_i^b\right)^T$, and $S_i^c = (w_i^c, v_i^c)^T$. The variables w_{2i-1}^a and w_{2i-1}^b are the same for the $Xaxis = (1,0,0)^T$, w_{2i}^a and w_{2i}^b are the same for the $Yaxis = (0,1,0)^T$, and w_i^c is $Zaxis = (0,0,1)^T$. In addition, $v_i^a = -w_i^a \times p_i^a$, $v_i^b = -w_i^b \times p_i^b$, and $v_i^c = (0,0,1)^T$, where $p_i^a = (0,0,2r)^T$ and $p_i^b = (0,0,0)^T$. The angle θ_i is the rotational pan joint angle and d is the distance between the frames $\{i_{down}\}$ and $\{i_{up}\}$. Finally, $[S]$ of $S = (w,v)^T$ is

$$[S] = \begin{bmatrix} [w] & v \\ 0 & 0 \end{bmatrix} \in se(3), \quad (6)$$

where

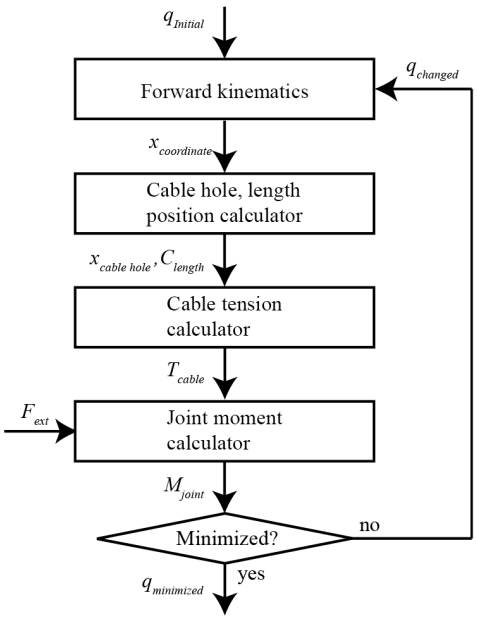

Figure 3. Algorithm to find the equilibrium position of the rolling joint by minimizing the joint moments.

$$[w] = \begin{bmatrix} 0 & -w_3 & w_2 \\ w_3 & 0 & -w_1 \\ -w_2 & w_1 & 0 \end{bmatrix} \in so(3). \quad (7)$$

Eight points configure the hole in the segment, and the positions p_j of these points are defined based on the position of the $\{i_{up}\}$ frame. The positions of the points P_i^j generated by the bending of the rolling joint are calculated in the fixed frame $\{s\}$ as

$$P_i^j = R_i^{T(\theta)} p_j + P_i^{T(\theta)}, i = 1, \dots, n, \text{ and } j = 1, \dots, 8, \quad (8)$$

where $R_i^{T(\theta)}$ and $P_i^{T(\theta)}$ are obtained by $T_i(\theta)$ as

$$T_i(\theta) = \begin{bmatrix} R_i^{T(\theta)} & P_i^{T(\theta)} \\ 0 & 1 \end{bmatrix} \in SE(3). \quad (9)$$

B. *Statics of the rolling joint*

The equilibrium position of the rolling joint is derived from statics. Since the thin cables are extended by tension, the equilibrium position of the rolling joint differs from the position derived by the kinematic model. As the cable lengths change, the cable tensions also change. In turn, the cable tension affects the joint moment and equilibrium position of the manipulator.

We modeled the cable as a linear spring to calculate the tension in the cable. The cable stiffness k_{cable} is derived using the cable initial length l_{ini} from the actuator to the end effector, the diameter D of the cable, and Young's modulus E of the cable:

$$k_{cable} = \frac{ED^2\pi}{4l_{ini}}. \quad (10)$$

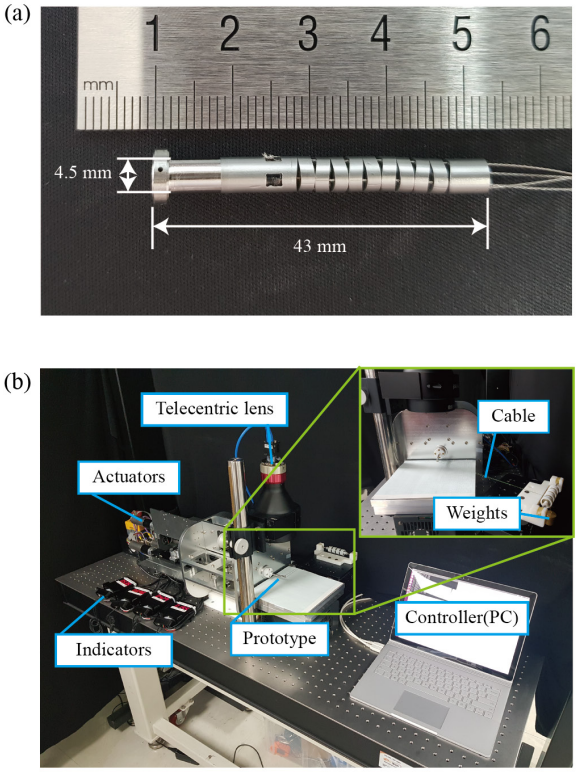

Figure 4. (a) Prototype of the rolling joint and (b) experimental setup for driving the prototype.

The tension in the cable, T_{cable}, is computed using the pretension $T_{pre,cable}$ and the difference in cable length due to the change in the posture of the rolling joint:

$$T_{cable} = T_{pre,cable} + k_{cable}(l_{change} - l_{base}). \quad (11)$$

Here, l_{change} is the cable length calculated from the changed position of the rolling joint, and l_{base} is the cable length based on the kinematic model of the rolling joint. While the cable can pull, it cannot push; if T_{cable} is negative, the cable tension is set zero. The joint moment M_i^{joint} is obtained by

$$M_i^{joint} = \sum_{j=1}^{4} P_{cable,j} \times T_{cable,j} + P_{ext} \times F_{ext}, \quad (12)$$

where $P_{cable} \in 3 \times 1$ is the position of the contact point between the cable and the i-th segment based on the center of the contact line, and $P_{ext} \in 3 \times 1$ is the position of the end effector applied by an external force based on the center of the contact line. Since each joint can only rotate in one direction, the joint moments calculated from (12) are removed, except for the moments in the same direction as the joint rotation.

C. *Optimization for minimizing the joint moments*

Due to the nonlinearity of the rolling joint, we chose the method of finding the equilibrium position by minimizing the joint moments, rather than directly calculating the static formula. If the joint moment of the rolling joint is minimized, the optimized position is the equilibrium position of the rolling joint. Fig. 3 shows the algorithm we used for determining the equilibrium position, which we now describe.

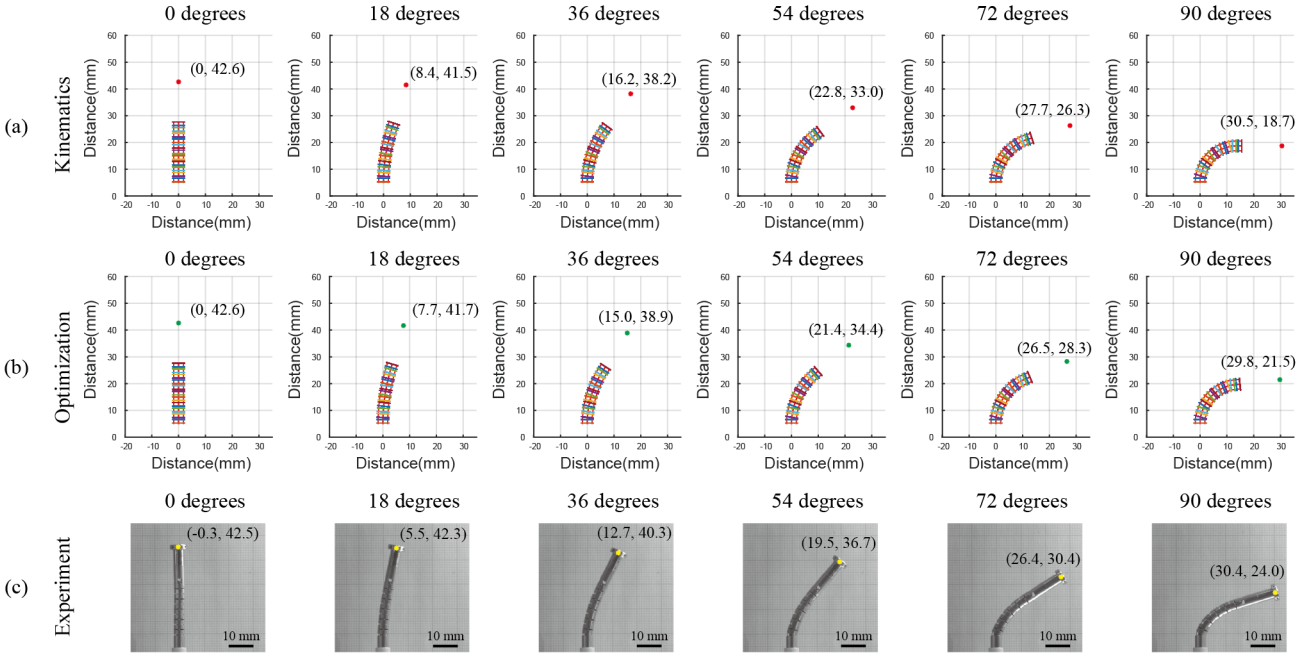

Figure 5. Bending motion of the rolling joint from 0-90 degrees. Position and shape (a) based on the kinematics, (b) based on the optimization, and (c) captured from images during the experiment using the prototype of the rolling joint. The yellow dot marks the end effector position.

First, the initial joint angle determines the position and orientation of the rolling joint segment. This position and the orientation of the segment determine the position of the cable hole and the cable length. Second, the cable length determines the cable tension, and the cable tension and external force determine the joint moment of the rolling joint. Third, if the statically calculated joint moment is not minimized, the calculation is repeated until the joint moment is minimized. When the joint moment is minimized, the equilibrium position is derived, as shown in Fig. 3.

We simulated the optimization simulation to minimize the joint moments by sequential quadratic programming (SQP) using Matlab's *fmincon* function. We used the joint angles as the design parameters of the optimization, the object function for which is expressed as:

$$min \sum_{i=1}^{n} \left| M_i^{joint} \right|. \tag{13}$$

Since the joint moments are in both positive and negative directions, simply summing the joint moments misrepresents their magnitudes. Therefore, we used the sum of the absolute values of the joint moments as the objective function to minimize the magnitude of the joint moments.

III. Experimental Results

We fabricated a stainless steel prototype of the rolling joint, as shown in Fig. 4(a). The diameter of the prototype is 4.5 mm, and the length of the prototype is 43 mm. The radius of the rolling surface of the segment is 7 mm. The number of the segments is 11, including the proximal and end segments. There are five pan joints and five tilt joints. By constructing the same number of joints and the segment's lengths, the prototype has the same bending motions in the up, down, left, and right directions. The cable hole has a diameter of 0.4 mm and is located at a distance of 1.8 mm from the center of the segment. The end effector is 15 mm from the distal joint, which is considered the location of the surgical instrument. In addition, the end effector is 7 mm in diameter and has a hole designed for a cable that only pulls the end effector. The cable diameter is 0.228 mm, and we cut the cable to be 350 mm long. The cable is made of stainless steel and manufactured by Carl Stahl (part number: 2009). The available bending angle of the prototype was set to $\pm 90^\circ$. The available strength of this cable is 4.54 kgf.

The experimental equipment is shown in Fig. 4(b). We used a laptop as the main controller to drive the prototype with sampling time of 10 ms. We used an EPOS4 50/5 manufactured by Maxon as the position controller for the linear actuators. The communication type was a controller area network (CAN). The linear actuators to drive the prototype were composed of a brushless DC motor manufactured by Maxon (part number: 539487) and a linear guide manufactured by Misumi (part number: LX1502C). We used a load cell manufactured by Dacell (part number: UU3-K20) and an indicator manufactured by Das (part number: Dscale2) to measure the feedback of the cable tension. The external force on the end effector was implemented using a weight attached to the cable. We obtained the shape and position of the prototype using a telecentric lens and camera manufactured by Edmund optics (part numbers 58259 and EO-1312, respectively).

We simulated the bending motion of the rolling joint using two models. The bending motion was the same in all directions, so the simulation and experiments were performed in one direction. One model was based on the kinematic model that assumes all joint angles are equal (see Fig. 5(a)). The other was constructed by finding the equilibrium position using the minimization of the joint moment, as shown in Fig. 5(b). We obtained the position and shape of the end effector at six

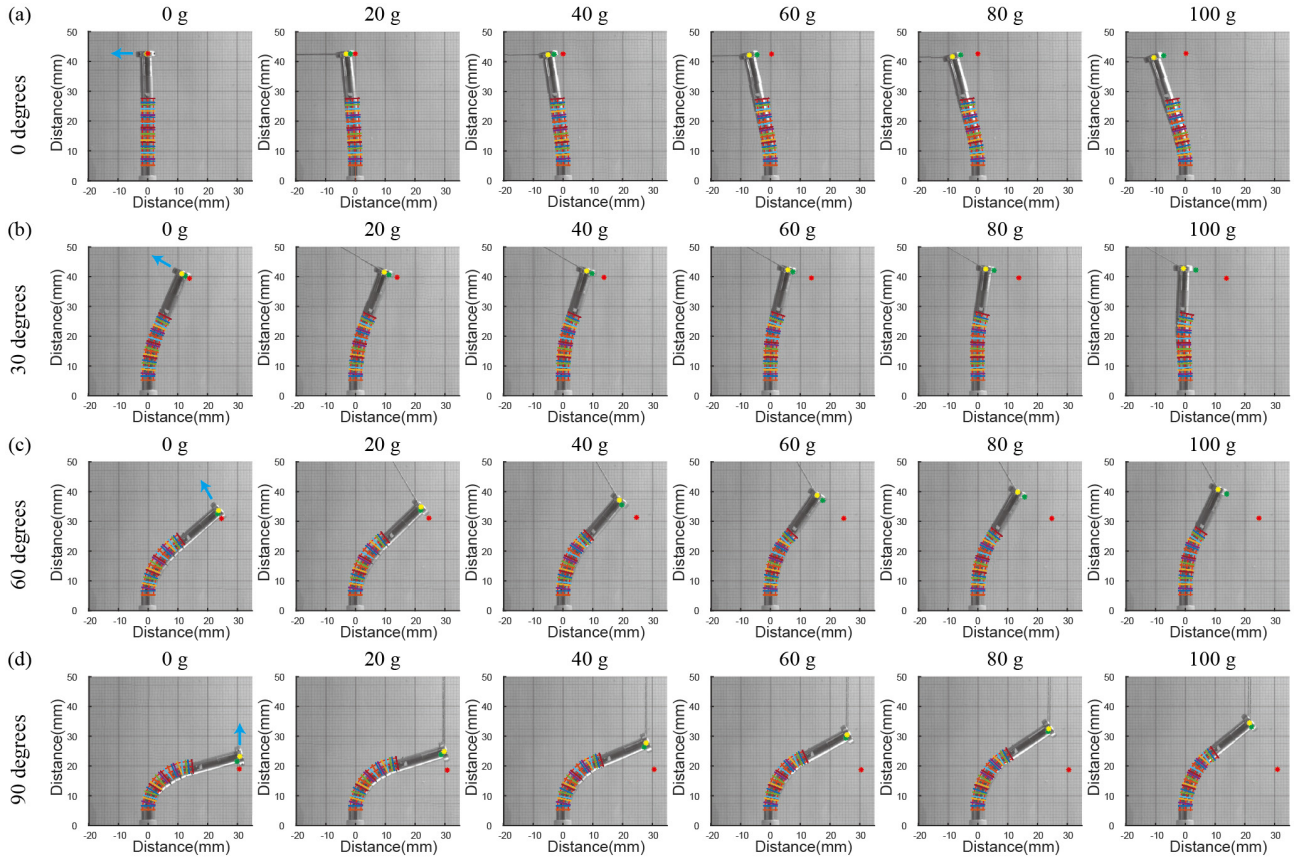

Figure 6. Position and shape of the end effector from simulations (colored lines) and experimental results (images) in which both the bending angle (y-axis) and external force (x-axis) are changed. The positions of the end effector in the optimized simulation results (marked by a green dots) are added to the images using the same scale and base position. The red dots are the end effector positions calculated based on the kinematics, and the yellow dots are the prototype's end effector positions. The external force is perpendicular to the direction in which the rolling joint is pointed (marked by the blue arrows in the first column). The bending angles are (a) 0 degrees, (b) 30 degrees, (c) 60 degrees, and (d) 90 degrees.

bending angles separated by 18 degrees from 0 to 90 degrees. We determined that the model based on the optimization bent less than did the model based on the kinematics. This implies that the rolling joint does not bend to the desired position derived by the kinematics when there is no external force.

Furthermore, we bent the prototype from 0 to 90 degrees using the actuation module in the absence of an external force. We captured images of the prototype and marked the end effector position by a yellow dot, as shown in Fig. 5(c). The prototype did not bend to the desired position based on the kinematics, similar to the simulation result shown in Fig. 5(b). The end effector of the prototype was bent less than the end effector in the optimized simulation because the cable tension was reduced by the friction between the cable and the segment. The end effector position of the simulation based on the optimization was closer to the position of the experimental result than that of the simulation based on the kinematics.

We then carried out experiments to bend the prototype of the rolling joint in the presence of an external force. The bending angles of the rolling joints were set to 0, 30, 60, and 90 degrees. The external force acting on the prototype was implemented by pulling the cable. The magnitude of the external force was changed by hanging different weights at the end of the cable. For each bending angle, the weight of the external force was increased from 0 to 100 g in 20 g increments. The external force acted on the end effector in a direction perpendicular to the direction that the rolling joint was pointed. For each combination of external force magnitude and bending angle, we captured images of the shape of the prototype and marked its end effector positions, as shown in Fig. 6.

To compare the simulation and the experimental results, we overlaid the shape of the optimized simulation onto the images of the experiment and marked the end effector positions as green dots, as shown in Fig. 6. In that figure, we also marked the end effector positions calculated by the kinematics as red dots. By comparing the shapes of the rolling joint from the optimized simulation and the prototype with the external force applied, it is apparent that both shapes were similar at each bending angle shown in Fig. 6. As the force increases in both the simulation and the experiment results, the rolling joint is pushed backward in the direction of the external force.

We compared the end effector positions between the simulation results and the experimental results. For a given bending angle, the positions calculated by the kinematics do not change as the external force increases. By contrast, the end effector positions of the optimized simulation and the experiment changed significantly (by more than 10 mm in some cases) as the external force increased. The end effector positions derived by the optimized simulation were similar to

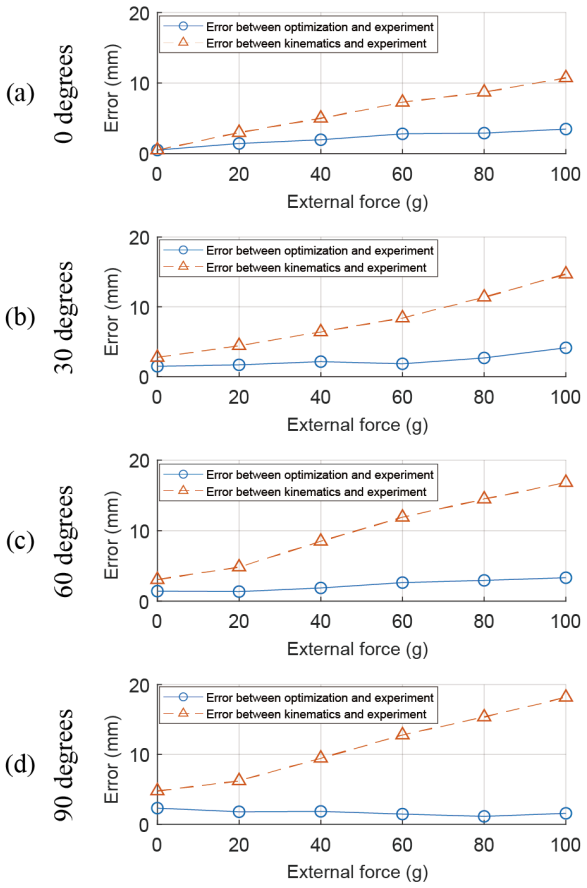

Figure 7. Errors between the simulations and experimental results as a function of bending angle: (a) 0 degrees, (b) 30 degrees, (c) 60 degrees, and (d) 90 degrees. The blue solid line with circles is the error between the optimized simulation and the experimental results, and the red dotted line with triangles is the error between the kinematic simulation and the experimental results.

those from the experimental results, even as the external force changed for the same bending angle.

Fig. 7 shows the error of the end effector positions, defined as the difference between the simulations and experimental results. The solid blue line with circles is the error between the optimized simulation and the experimental results, and the dotted red line with triangles is the error between the kinematics simulation and the experimental results. The figure demonstrates that the errors of the kinematics simulation increase monotonically with bending angle, while the errors of the optimized simulation remain relatively constant.

The average error between the optimized simulation and the experimental results is 2.11 mm, and the maximum error is 4.13 mm. By contrast, the average error between the kinematics simulation and the experimental results is 8.73 mm, and the maximum error is 18.17 mm. Therefore, with optimization, the average error is reduced by 75.74%, and the maximum error is reduced by 77.22%. These results demonstrate that the optimized simulation accurately estimates the shape and position of the rolling joint when the bending angle and external force are changed.

IV. Conclusion

In this paper, we presented an optimization method to find the equilibrium position of the rolling joint in HRMs. The latter was found by minimizing the sum of the absolute values of the joint moments. The error between the optimized simulation and the experiment results was less than 4.13 mm, which was 77.22% better than the kinematic simulation that assumed all joint angles are equal. The way that the shape of the rolling joint changed in the optimized simulation was very similar to the way that the shape of the experimental prototype changed. This verifies that our method for finding the equilibrium position accurately estimates the bending movement of the rolling joint in the presence of an external force.

Our method for estimating the shape and position of the rolling joint can be applied to HRMs with multi-segments, which is not limited to the rolling joint. On the other hand, our study has a limitation that it is difficult to control in real-time because it requires sufficient time for the optimization.

We believe this study is the starting point for future research on the control technology of HRMs for the automation of microsurgical robots. In future work, if the optimization calculation speed is fast, and the sensor attached to the tip observes the reaction force, this study will contribute to the real-time control and the automation of the surgical robots.

References

[1] V. Vitiello, S. L. Lee, T. P. Cundy, and G. Z. Yang, "Emerging robotic platforms for minimally invasive surgery," *IEEE Rev. Biomed. Eng.*, vol. 6, pp. 111–126, 2013.

[2] J. Shang *et al.*, "Design of a multitasking robotic platform with flexible arms and articulated head for Minimally Invasive Surgery," *IEEE Int. Conf. Intell. Robot. Syst.*, pp. 1988–1993, 2012.

[3] C. C. Thompson, M. Ryou, N. J. Soper, E. S. Hungess, R. I. Rothstein, and L. L. Swanstrom, "Evaluation of a manually driven, multitasking platform for complex endoluminal and natural orifice transluminal endoscopic surgery applications (with video)," *Gastrointest. Endosc.*, vol. 70, no. 1, pp. 121–125, 2009.

[4] A. Degani, H. Choset, B. Zubiate, T. Ota, and M. Zenati, "Highly articulated robotic probe for minimally invasive surgery," *Proc. 30th Annu. Int. Conf. IEEE Eng. Med. Biol. Soc. EMBS'08 - "Personalized Healthc. through Technol.*, no. May, pp. 3273–3276, 2008.

[5] J. Kim, S. Kwon, and K. Kim, "Novel block mechanism for rolling joints in minimally invasive surgery," *Mech. Mach. Theory*, vol. 147, p. 103774, 2020.

[6] P. Berthet-Rayne, K. Leibrandt, K. Kim, C. A. Seneci, J. Shang, and G.-Z. Yang, "Rolling-joint design optimization for tendon driven snake-like surgical robots," in *2018 IEEE/RSJ International Conference on Intelligent Robots and Systems (IROS)*, 2018, pp. 4964–4971.

[7] M. C. Lei and R. Du, "A study on the bending mechanism of the flexible ureteroscope," *ICCAS 2010 - Int. Conf. Control. Autom. Syst.*, pp. 2019–2023, 2010.

[8] S. Song, Z. Li, M. Q. H. Meng, H. Yu, and H. Ren, "Real-time shape estimation for wire-driven flexible robots with multiple bending sections based on quadratic Bézier curves," *IEEE Sens. J.*, vol. 15, no. 11, pp. 6326–6334, 2015.

[9] W. Xu, T. Liu, and Y. Li, "Kinematics, Dynamics, and Control of a Cable-Driven Hyper-Redundant Manipulator," *IEEE/ASME Trans. Mechatronics*, vol. 23, no. 4, pp. 1693–1704, 2018.

[10] Y. J. Kim, S. Cheng, S. Kim, and K. Iagnemma, "A stiffness-adjustable hyperredundant manipulator using a variable neutral-line mechanism for minimally invasive surgery," *IEEE Trans. Robot.*, vol. 30, no. 2, pp. 382–395, 2014.